IEEE Access
Multidisciplinary | Rapid Review | Open Access Journal

Received 10 October 2023, accepted 4 November 2023, date of publication 9 November 2023,
date of current version 16 November 2023.

Digital Object Identifier 10.1109/ACCESS.2023.3331686

APPLIED RESEARCH

Refined Critical Plane Methodology for Predicting Fretting Fatigue Crack Initiation Based on Shear Strain Dynamics

WEN ZHOU[1], JIANGANG YE[1], KUN MAO[2], ZHENJIE LIU[1], AND SHANG XIA[1], (Member, IEEE)
[1]Quzhou Special Equipment Inspection Center, Quzhou 324000, China
[2]Faculty of Information Engineering, Quzhou College of Technology, Quzhou 324000, China

Corresponding author: Jiangang Ye (13957003252@163.com)

This work was supported in part by the Zhejiang Provincial Administration for Market Regulation Research Project of China under Grant ZC2021B091, and in part by the Quzhou Science and Technology Key Project of China under Grant 2023K247 and Grant 2023K044.

ABSTRACT The present study posits that variations in maximum shear strain energy are the principal determinants for the onset of fretting fatigue cracks. We propose a refined critical plane methodology, termed the shear stress-strain interaction (SSI) critical plane method, predicated on shear strain, for predicting fretting fatigue crack initiation characteristics. The novelty of this methodology resides in its focus on cyclic shear strain as the genesis of crack initiation. To verify the effectiveness of the SSI critical plane method, finite element analyses using ANSYS were executed on fretting bridge and pad models to quantify the SSI interaction parameters. A comprehensive evaluation against established metrics-maximum shear range, stress-weighted tangential parameters, and fretting parameters was undertaken. The findings, in alignment with extant experimental data, confirm the robustness of the proposed method.

INDEX TERMS Fretting fatigue, fretting pad, fretting bridge, crack initiation, SSI critical plane method.

I. INTRODUCTION

Fretting fatigue encompasses issues related to fatigue strength and the resilience of components under fretting-induced wear [1]. Such conditions can expedite the early onset and rapid propagation of fatigue cracks, ultimately culminating in component failure, often well below the material's established fatigue limit or even beneath its elastic limit. These failures are evident in various structural elements such as bolt connections, tenon joints, rivets, lifting steel wires, and overhead lines [2].

The critical plane method identifies a specific plane within a physical specimen where crack initiation and propagation occur. Researchers determine the initiation and progression of cracks based on the stress and strain experienced on this designated plane [3], [4], [5], [6], [7]. Notable contributions to this methodology were made by Brown and Mille [8], who initially introduced a combination of the maximum shear strain range and the maximum normal tensile strain on the maximum shear plane in multiaxial fatigue. This provided a fundamental explanation for the mechanism of fretting crack propagation.

Subsequent studies on fretting sphere models by Lykins, Szolwinski, and Farris led to the proposal of critical plane methods based on maximum shear range (MSR) [9], [10], a modified Smith-Watson-Topper (SWT) approach [11] and Findley (F) parameters [12], respectively. Rangel et al. [13] suggested an iterative model calibrated with the fatigue stress-strain life curve for determining the initiation and total life of fretting fatigue cracks, utilizing SWT to establish the crack initiation path.

Further advancements were made by Wang et al. [14], who explored fretting crack propagation using the maximum tangential stress criterion and its extensions, incorporating contact stress between crack surfaces and conducting numerical analyses of crack propagation. Dong et al. [15], integrating the critical distance theory, employed improved Dang Van and McDiarmid criteria alongside SWT as multiaxial fatigue criteria to assess fretting fatigue crack initiation.

The associate editor coordinating the review of this manuscript and approving it for publication was Eric Li.

Deng et al. [16] delved into the impact of the size and position of a single critical micropore on the lifespan of heterogeneous material fretting fatigue, utilizing numerical simulations and a revised critical plane criterion.

With the advent of computational capabilities, scholars have leveraged big data and neural networks to forecast the fretting fatigue lifespan. Han et al. [17], [18], [19], [20] utilized deep neural networks with F parameters to enhance the precision of predicting the fretting fatigue crack initiation lifespan. It is important to note that these methods still rely on the initial three critical plane parameters.

However, the MSR and F parameters necessitate calibration using actual general fatigue experimental data, rendering them semi-empirical formulas with limited universality. Meanwhile, the SWT critical plane method solely considers the influence of normal stress on fretting fatigue, overlooking the effect of shear stress. Thus, this article proposes an improved critical plane method for predicting the characteristics of fretting fatigue crack initiation based on shear strain. This approach underscores that fluctuations in maximum shear strain energy can lead to the generation of fretting fatigue cracks. This is one of the energy methods in fretting fatigue initiation prediction, which does not need more fatigue experimental data. The implications of this method are of considerable significance, particularly in averting catastrophic accidents stemming from fretting fatigue in real-world engineering applications.

II. CRITICAL PLANE METHOD

A. DERIVATION OF THE STRESS–STRAIN INTERACTION CRITICAL PLANE METHOD

In alignment with the characteristics of fretting fatigue, the fretting fatigue process entails the application of a normal load to the top of the fretting pad while the failed component is subjected to axial forces. At the contact interface, various stress components, encompassing normal, axial, and tangential stresses, come into play. Fretting cracks initiate and propagate through cyclic processes of maximum and minimum shear strains, as well as cyclic processes of maximum and minimum normal strains. According to theories postulated by Brown, Miller, and others, cyclic shear strains predominantly catalyze crack initiation, whereas cyclic normal strains are the primary driving force behind crack propagation.

In the context of fretting fatigue failure, it is notable that the initiation of fretting cracks accounts for approximately 89% of the entire failure process, with the subsequent crack propagation to ultimate failure constituting only approximately 11% [21]. Consequently, in the prediction process, it is prudent to consider the crack initiation phase as the entirety of the specimen's failure process.

From the aforementioned theoretical framework, it becomes evident that fretting fatigue crack initiation is primarily induced by cyclic maximum and minimum shear strains. The maximum shear strain characterizes these cracks initiated on the plane. So fluctuations in maximum shear strain energy

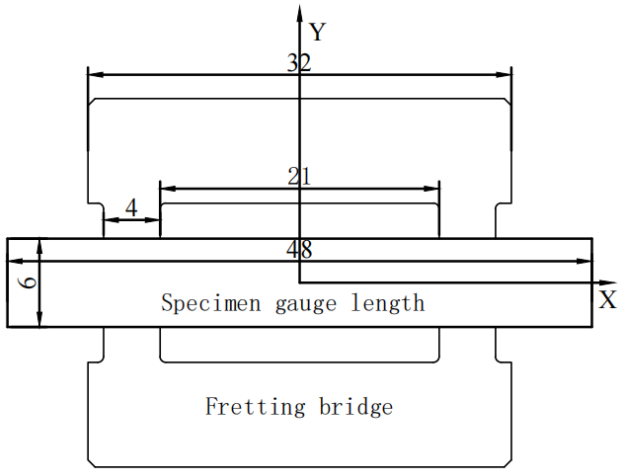

FIGURE 1. Fretting bridge geometric model.

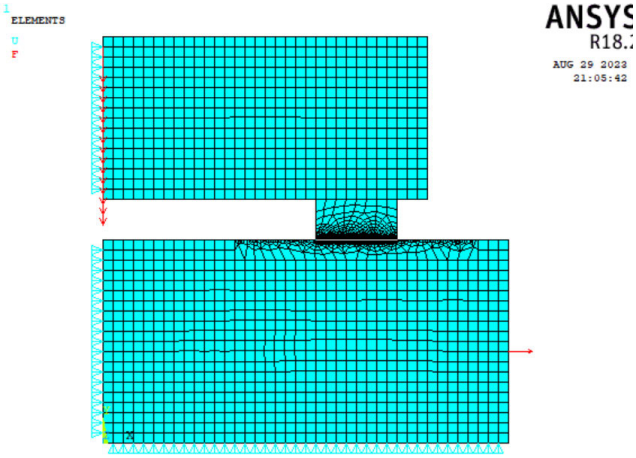

FIGURE 2. Fretting bridge finite element loading diagram.

emerge, which can lead to the generation of fretting fatigue cracks. Building upon this comprehension, a critical interface approach, known as the stress-strain interaction (SSI) critical interface method, is introduced. This method is designed to ascertain the location and orientation of fretting crack initiation.

In accordance with the concept of plane stress, consider a thin plate subjected to tensile stresses σ_x, σ_y and shear stress τ_{xy} on each side. The stresses acting on the surface of the plate can be regarded as negligible with $\sigma_z = \tau_{xz} = \tau_{yz} = 0$.

Static balance can be utilized to determine the stress behavior on a plane that forms an angle θ counterclockwise with respect to the y-axis. The coordinate transformation equations are as follows:

$$\sigma_\theta = \frac{\sigma_x + \sigma_y}{2} + \frac{\sigma_x - \sigma_y}{2}\cos(2\theta) + \tau_{xy}\sin(2\theta) \quad (1)$$

$$\tau_\theta = \frac{\sigma_x - \sigma_y}{2}\sin(2\theta) - \tau_{xy}\cos(2\theta) \quad (2)$$

According to the relationship of stress and strain:

$$\gamma_\theta = (\varepsilon_x - \varepsilon_y)\sin 2\theta + \gamma_{xy}\cos 2\theta \quad (3)$$

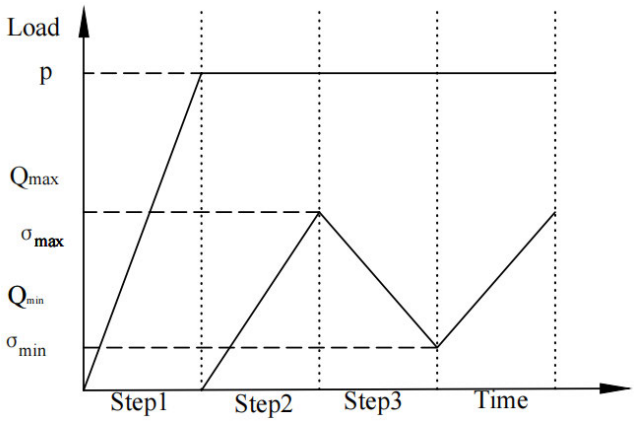

FIGURE 3. Loading process diagram.

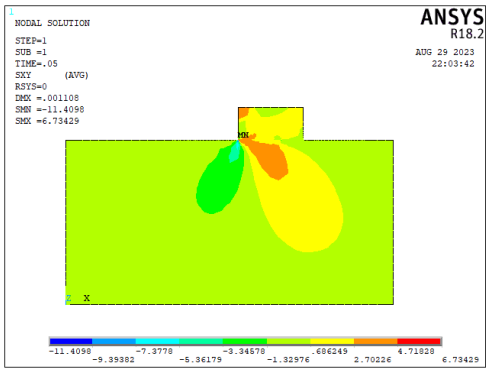

FIGURE 4. Shear stress diagram in the XY direction during the first load step.

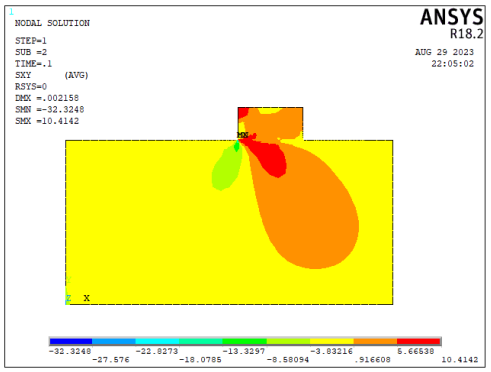

FIGURE 5. Shear stress diagram in the XY direction during the second load step.

where σ_x, σ_y, τ_{xy}, ε_x, ε_y, and γ_{xy} represent the stress and strain values at the respective node.

As elucidated in the preceding discussion, the inception of fretting fatigue cracks primarily arises from cyclic variations in maximum and minimum shear strains. Hence, it is reasonable to postulate that the critical plane at the site of fretting fatigue initiation corresponds to where the disparity in shear strain achieves its utmost under the influence of maximum and minimum loads, expressed as:

$$\Delta\gamma = \gamma_{\max} - \gamma_{\min} \tag{4}$$

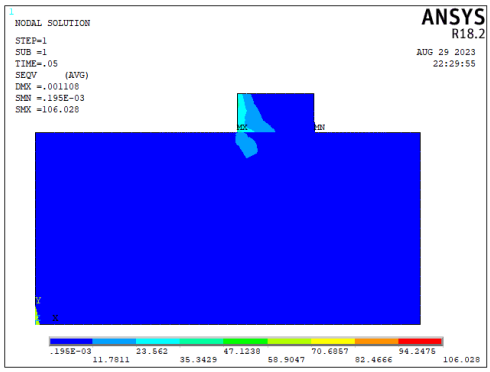

FIGURE 6. von-Mises stress diagram during the first load step.

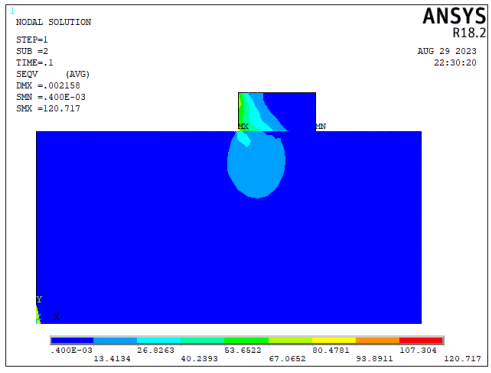

FIGURE 7. von-Mises stress diagram during the second loading step.

Here, $\gamma_{\max}$ and $\gamma_{\min}$ denote the range of strains under the influence of maximum and minimum loads, respectively.

Consequently, the shear strain energy, denoted as SSI, can be conceptualized as the product of the maximum shear strain energy and the maximum shear strain occurring on the critical plane, as articulated in:

$$SSI = \frac{\Delta\gamma}{2}\tau_{\max} \tag{5}$$

B. OTHER METHODS

1) MSR PARAMETERS

Lykins et al. [9], [10] acquired plane fatigue life data under varying stress ratios through experimental means, confirming the anticipated substantial impact of nominal stress and strain on titanium alloy materials. To evaluate the effect of the initial shear stress ratio on the critical plane, Lykins and his team employed the integration equation proposed by the Walker method. This integration resulted in the introduction of the MSR critical plane parameters, as exemplified in Equation 6:

$$MSR = \Delta\tau_{crit} = \tau_{\max}(1 - R_\tau)^m \tag{6}$$

where $\tau_{\max}$ represents the maximum shear stress on the critical plane and R_τ signifies the shear stress ratio on the critical plane.

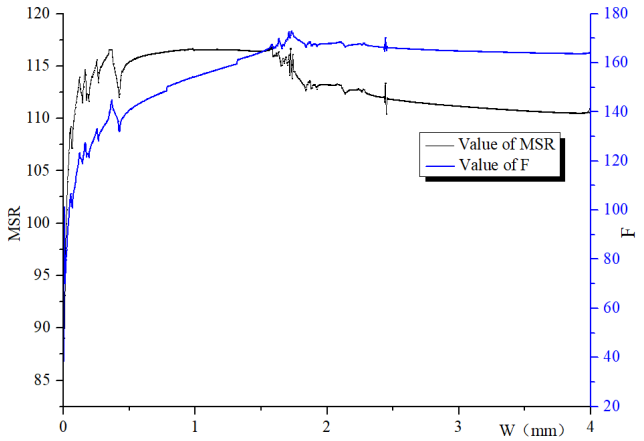

FIGURE 8. Distribution of the MSR and F values along the bridge foot.

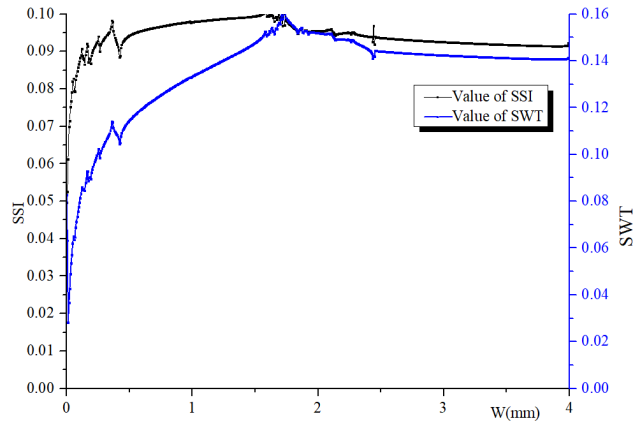

FIGURE 9. Distribution of SWT and SSI values along the bridge foot.

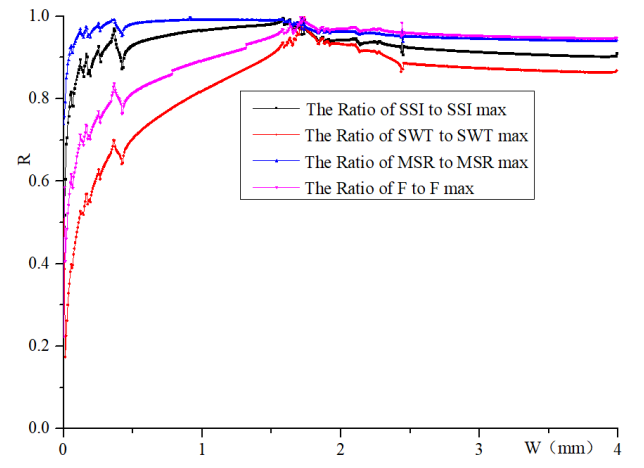

FIGURE 10. Distribution of the ratio of each parameter to its maximum value along the bridge foot.

2) SWT PARAMETERS

Szolwinski et al. [11] employed Basquin's equation to derive the SWT parameters from the strain-life equation, considering the maximum stress and strain amplitude. They introduced fretting fatigue parameters based on the SWT critical plane, as depicted in Equation 7:

$$SWT = \sigma_{\max} \Delta\varepsilon_a \tag{7}$$

where $\Delta\varepsilon_a$ denotes the maximum value of the strain amplitude difference under the effect of maximum and minimum loads, and $\sigma_{\max}$ represents the maximum stress value on the plane with the maximum $\Delta\varepsilon_a$ value.

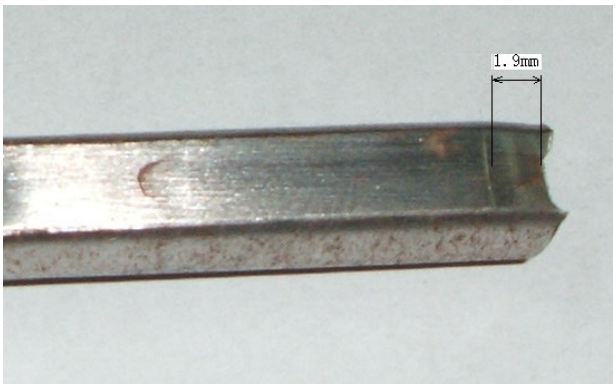

FIGURE 11. Fretting fatigue sample fracture position diagram.

3) F PARAMETER

F Parameter, introduced by Findley WN [12], encompasses the effects of shear stress and normal stress on fretting fatigue cracking, expressed as in equation 8:

$$F = \Delta\tau + k \cdot \sigma_n^{\max} \tag{8}$$

The critical plane for F is where the maximum value of F is attained, and the k value is known to be 0.35 from previous research. In contrast to the parameters mentioned earlier, the F parameter is based on the mixed normal and shear stresses on the critical plane.

III. COMPARATIVE ANALYSIS OF THE CRACK INITIATION CHARACTERISTICS

A. COMPARATIVE ANALYSIS OF CRACK INITIATION CHARACTERISTICS IN THE FRETTING BRIDGE MODEL

The geometry of the fretting bridge model is depicted in Figure 1, featuring a fretting bridge length of 32 mm, a foot width of 4 mm, a sample length of 48 mm, and a width of 6 mm, specified in a two-dimensional orientation as shown in the diagram. The fretting bridge and the sample material are constructed from #45 steel, with its elastic modulus denoted as $E = 210GPa$, $\mu = 0.3$.

Given the model's symmetry to the X and Y axes, it allows for the analysis of only a quarter of the model. The simulation employs the face-to-face contact method within ANSYS finite software for computation. As the material of the fretting bridge matches that of the sample, a flexible-to-flexible contact nonlinear simulation method is chosen. The model utilizes plane82 elements, with the contact surface

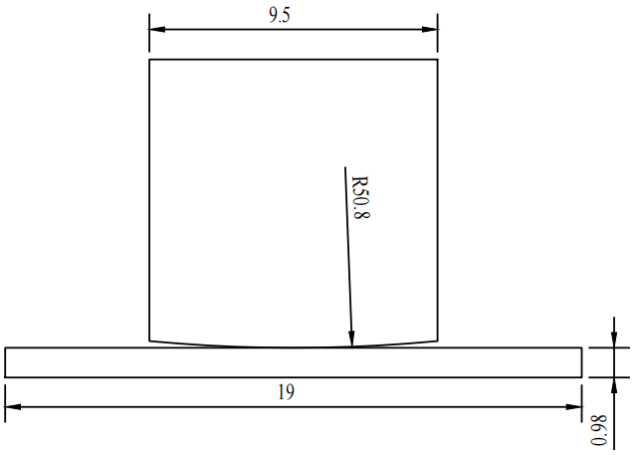

FIGURE 12. Simplified schematic of the cylindrical and planar contact calculation.

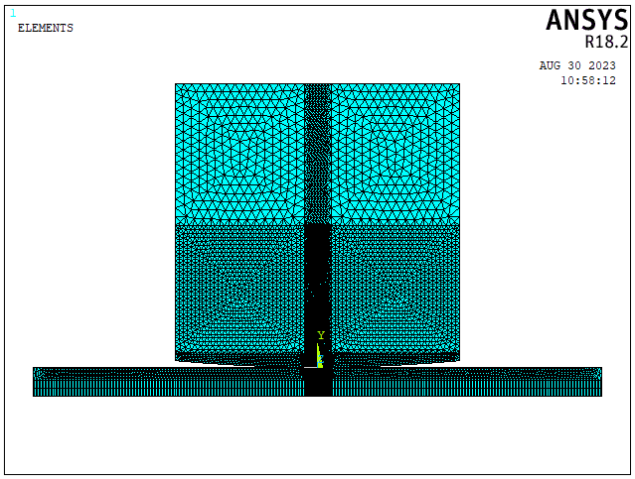

FIGURE 13. ANSYS mesh division diagram.

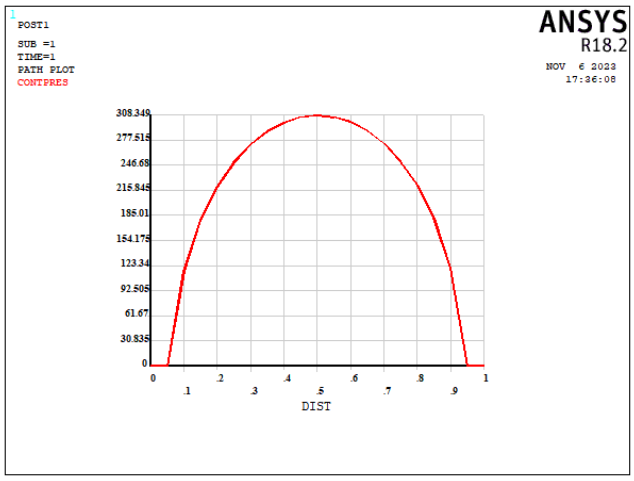

FIGURE 14. Calculation of contact surface width.

divided into ''conta172'' elements and the target surface into ''targe169'' elements.

Drawing from the insights of previous researchers, it is established that mesh refinement is essential in the contact region between the fretting bridge and the sample. Mesh sizes smaller than 10 μm are deemed sufficient for this purpose [22], [23]. Consequently, a finite element mesh with a size of 6 μm is chosen for the contact part. This involves quadrilateral mesh division in the contact area and free mesh division in the transition area, ensuring both computational precision and a manageable computational load. The mesh model encompasses a total of 29,636 nodes and 30,146 elements, including 1,000 contact elements and 800 target elements, as visualized in Figure 2.

Symmetric constraints are imposed on the left side of the fretting bridge and the lower end of the sample, as illustrated in Figure 3. In this configuration, a normal load of 1440 N is considered, along with an axial cyclic load of 240 MPa and a stress ratio of 0, serving as an illustrative example.

The finite element nonlinear calculations unveil the distribution of shear stresses in the xy direction, and von-Mises stresses during the initial and subsequent load steps, as illustrated in Figures 4 to 7. These figures clearly demonstrate that the highest magnitudes of both shear stresses in the xy direction and von-Mises stresses are localized at the inner edge, precisely where the fretting foot comes into contact with the sample. Additionally, they extend at a particular angle into the sample.

Based on the previous simulation computations, the values of stresses and strains in the x direction, stresses and strains in the y direction, and shear stresses and shear strains in the xy direction under both maximum and minimum cyclic axial loads were determined. Utilizing the MSR, SWT, F, and SSI computational formulas, it becomes feasible to calculate the distribution of various parameter values along the width of the bridge foot, as illustrated in Figures 8 to 10. In these figures, ''W'' represents the width of the bridge foot, while ''R'' denotes the ratio of the distribution of SSI, SWT, MSR, and F along the bridge foot to their maximum value. From these figures, it is discernible that the parameters attain their maximum values in the vicinity of positions 1.72 to 1.73 of the bridge foot width, signifying that the initiation of fretting cracks takes place near the contact edge.

Drawing from experimental results conducted by Sun Weiming at the Chemical Machinery Research Institute of Zhejiang University of Technology, employing the micro-controlled electrohydraulic servo static–dynamic material testing machine EHFED250kN-40 L manufactured by Shimazu Company in Japan, the analysis of fracture locations across all tested samples reveals that the onset of fretting wear micro-cracks occurs near the contact edge, approximately 1.9 mm from the inner contact edge, as depicted in Figure 11 [24]. The comparison between the predicted positions and the experimental findings demonstrates the concurrence between the theoretical predictions derived

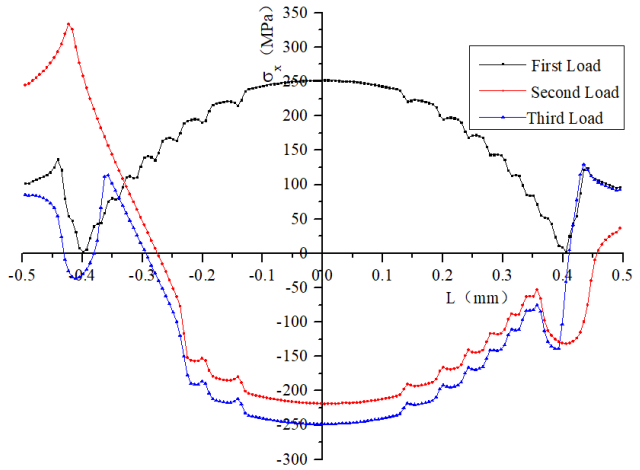

FIGURE 15. Stress diagram of each loading step in the X direction on the contact surface.

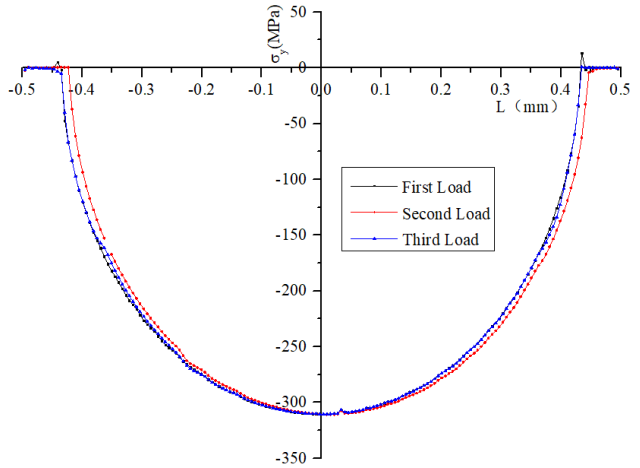

FIGURE 16. Stress diagram of each loading step in the Y direction on the contact surface.

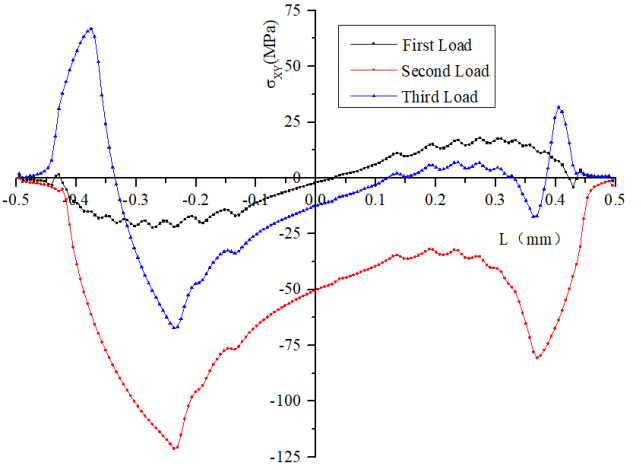

FIGURE 17. Shear stress diagram of each loading step in the XY direction on the contact surface.

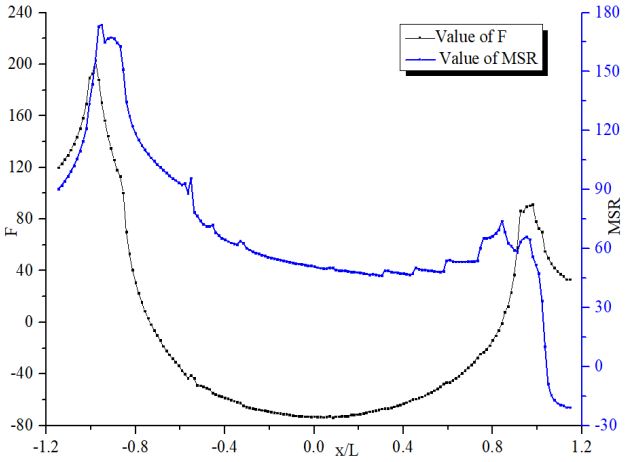

FIGURE 18. Distribution of MSR and F values along the contact surface.

from MSR, SWT, F, and SSI and the outcomes of the experiments.

In the calculation of the crack initiation angle, we determine the angle of the surface where the SSI reaches its maximum value at various nodes. This angle corresponds to the angle of the critical surface at the moment when the parameter achieves its peak value. Specifically, this angle varies from -45° to +45° in the normal direction. It is worth noting that this range aligns with the observed crack initiation angle variation of ±10° within the range of ±45° in experimental findings [9], [10]. This alignment underscores the significance of these four parameters in predicting the crack initiation angle.

B. COMPARATIVE ANALYSIS OF CRACK INITIATION CHARACTERISTICS IN THE FRETTING PAD MODEL

A fretting pad model encompassing a cylinder and a plane is formulated to enable a comparative analysis of the crack initiation location and direction using the SSI, MSR, F, and SWT methods. The model's configuration is illustrated in Figure 12, presenting the geometric dimensions suitable for a two-dimensional plane strain contact scenario. The material employed is Ti-6Al-4 V, characterized by an elastic modulus (E) of 127 GPa, $\mu = 0.3$.

ANSYS finite element software employs the face-to-face contact method for computations. Due to the substantial thickness of the fretting pad and the relatively low applied pressure, the cylindrical fretting pad can be treated as a rigid body without undergoing deformation. The simulation method involves selecting a flexible body and rigid body contact for nonlinear simulation.

The model is constructed using plane82 elements, with the contact surface subdivided into "conta172" elements and the target surface subdivided into "targe169" elements. As per the insights from previous scholarly research, it is established that the contact area between the fretting pad and the sample should undergo fine mesh division, with a grid size smaller than 10 μm considered sufficient for this purpose [22], [23]. Hence, for this instance, the finite element grid is set at 6 μm.

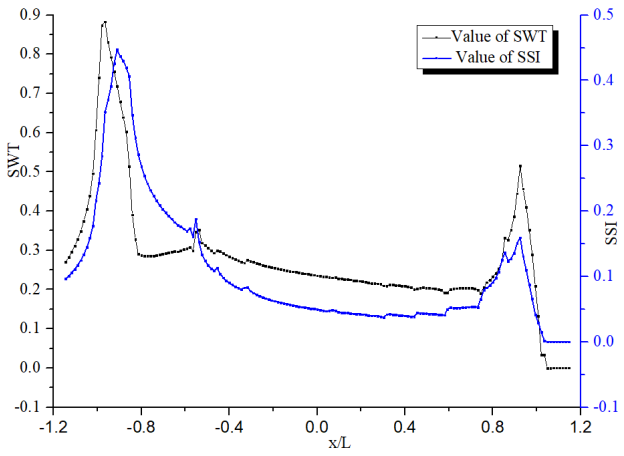

FIGURE 19. Distribution of SWT and SSI values along the contact surface.

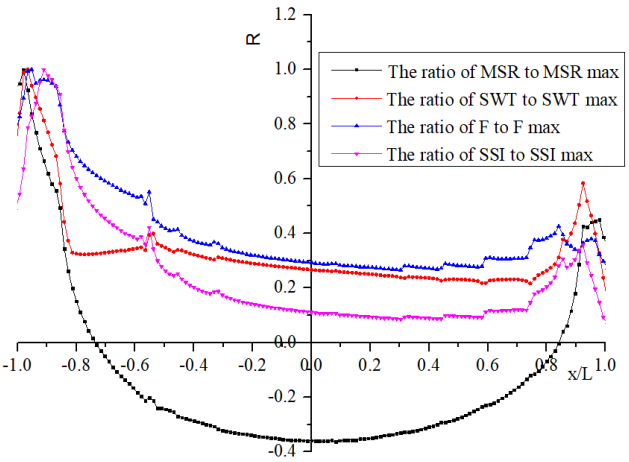

FIGURE 20. Distribution of various parameters to their maximum values along the contact surface.

To streamline the calculation process, the finite element grid becomes coarser as we move away from the contact area. Employing quadrilateral grid division in the contact area and triangular grid division in other regions fulfills the precision requirements of the computation. The model comprises a total of 111,054 nodes and 40,738 elements. Within the contact subunits, the lengths vary according to different regions, amounting to 40,295 contact units and 39,956 target units in total, as illustrated after grid division in Figure 13.

To prevent lateral movement of the fretting pad, a constraint in the x-direction is imposed on the right side of the pad, and a y-direction constraint is applied to the left side of the sample. Given that only half of the model is considered, a symmetrical constraint is applied at the lower end of the sample. An applied normal load of 210 N/mm is exerted on the upper end of the fretting pad, and the resulting data are presented in Figure 14. In Figure 14, the horizontal coordinate 0 corresponds to -0.5 in Figure 16, while the horizontal coordinate 1 corresponds to 0.5 in Figure 16. A total of 145 nodes are in contact on the contact surface, and through coordinate values, the contact surface width 'a' can be calculated as 0.87 mm. The finite element calculation results in Figure 14 reveal that the maximum contact pressure on the contact surface amounts to 308.349MPa.

In accordance with the semiwidth formula for the contact surface, the value of b can be calculated as follows:

$$b = 2\sqrt{\frac{2(1-\nu^2)}{\pi} \cdot \frac{PR}{E}} = 0.4412mm \tag{9}$$

This results in a contact surface width of 2b = 0.8824 mm.

Utilizing the maximum contact stress formula, P_{max} can be ascertained as:

$$P_{\max} = \sqrt{\frac{1}{2\pi(1-\nu^2)} \cdot \frac{PE}{R}} = 303.02MPa \tag{10}$$

This yields a maximum contact pressure of 303.02 MPa.

Comparing the finite element calculation results with the analytical formula, the error in the contact surface width is 1.4%. Meanwhile, the error in the maximum contact pressure is only 1.8%, demonstrating the feasibility of this finite element method.

To simulate the load, the following steps are undertaken:

Initially, a normal load is applied by adding a normal load of 210 N/mm to the upper end of the fretting pad.

Subsequently, the maximum axial load Q_max of 200 MPa is introduced. This load is specifically added to the right section of the sample.

Last, the minimum axial load Q_min is applied, with a stress ratio of 0.1 between the maximum and minimum loads during the loading process.

This loading process is graphically illustrated in Figure 3. Subsequent calculation yield stress diagrams for each loading step in the X direction on the contact surface, as well as in the Y and XY directions, are displayed in Figures 15 to 17. From these figures, it is evident that under the three types of loading steps, the stress in the X direction undergoes a sudden change at both contact edges. Furthermore, the stress in the X direction maintains a consistent trend during the second and third loading steps within the contact area. The stress diagrams in the Y direction exhibit a high degree of consistency.

Regarding the shear stress diagram in the XY direction, it becomes apparent that the contact edge serves as the starting point where the shear stress in the XY direction begins to increase or decrease. Under the condition of axial loading, specifically during the second and third loading steps, the shear stress in the XY direction maintains a consistent trend.

Utilizing the obtained stress values in the X and Y directions, as well as the shear stress values in the XY direction at different load steps, we can calculate the distribution of SWT, MSR, F, and SSI parameter values along the contact surface, as presented in Figures 18 to 20. In these figures, 'x/L' represents the ratio of each contact position to the width of the contact surface, while "R" denotes the ratio of the distribution of SSI, SWT, MSR, and F along the contact surface to their maximum value.

As observed in Figures 18 and 19, the maximum value of 'F' is situated at a position of -0.979, the peak of 'MSR' is at -0.951, the highest 'SWT' value occurs at -0.965, and the zenith for the 'SSI' parameter is found at -0.910. Additionally, Figure 20 illustrates that the peak value of each parameter, corresponding to the point where the ratio equals 1, falls within the range of -0.9 to -1. This alignment with the experimental findings of previous scholars [9], [25] indicates that the initiation of fretting fatigue cracks indeed takes place at the contact edge. This suggests that the 'SSI' parameter method fundamentally aligns with the 'MSR,' 'SWT,' and 'F' parameter methods in predicting the initiation location of cracks.

Furthermore, in the computation of the 'SSI' parameter, when reaching its maximum value, the corresponding critical face angle, specifically the angle with the normal direction, is determined to be 35°. This finding is consistent with experimental results [9], [10] where the initiation angle exhibited variations within ±45°, displaying a deviation of no more than ±10°.

IV. RESULTS

(1) Founded on the theory that fluctuations in maximum shear strain energy are the primary causative factor behind the emergence of fretting fatigue cracks, we have introduced an enhanced SSI critical plane method based on shear strain for predicting the characteristics of fretting crack initiation.

(2) Based on the fretting bridges model, this paper uses the plane critical method to calculate the distribution of MSR, SWT, F, and SSI parameter values along the width of the bridge foot. The crack initiation location prediction of the SSI parameter is near the contact edge, which is the same as the experimental results and aligns with the other three parameters, namely, MSR, SWT, and F.

(3)Based on the fretting pad model, the distribution of MSR, SWT, F, and SSI parameter values along the contact surface are calculated. The result of these four parameters concurs with prior research literature, which describes the initiation location of fretting cracks at the contact edge in the fretting pad model.

(4)The computation of crack initiation surface angles corresponding to the maximum values of SSI, known as the predicted crack initiation angles, is consistent with the variations observed by previous researchers. These variations typically fall within the range of ±45° with deviations up to ±10°.

REFERENCES

[1] H. Mingjian, *Fretting Fatigue of Component*. Beijing, China: National Defence Industry Press, (in Chinese), 1994.

[2] A. Omrani, L. Dieng, S. Langlois, and P. Van Dyke, "Friction properties at the contact interfaces of overhead line aluminium conductors," *IEEE Trans. Power Del.*, vol. 37, no. 1, pp. 442–448, Feb. 2022.

[3] C. Wang, D. Wang, and M. A. Wahab, "Fretting fatigue lifetime estimation for heterogeneous material using critical distance with mesh control," *Eng. Fract. Mech.*, vol. 281, Mar. 2023, Art. no. 109092.

[4] A. L. Pinto, R. Talemi, and J. A. Araújo, "Fretting fatigue total life assessment including wear and a varying critical distance," *Int. J. Fatigue*, vol. 156, Mar. 2022, Art. no. 106589.

[5] S. Vantadori, F. Abbasi, A. Zanichelli, D. Leonetti, G. P. Pucillo, and G. H. Majzoobi, "Influence of normal load frequency on fretting fatigue behaviour by a critical plane-based approach," *Int. J. Fatigue*, vol. 158, May 2022, Art. no. 106724.

[6] D. Infante-Garcia, A. Zabala, E. Giner, and I. Llavori, "On the use of the theory of critical distances with mesh control for fretting fatigue life assessment in complete and nearly complete contacts," *Theor. Appl. Fract. Mech.*, vol. 121, Oct. 2022, Art. no. 103476.

[7] S. Vantadori, G. M. J. Almeida, G. Fortese, G. C. V. Pessoa, and J. A. Araújo, "Early fretting crack orientation by using the critical plane approach," *Int. J. Fatigue*, vol. 114, pp. 282–288, Sep. 2018.

[8] M. W. Brown and K. J. Miller, "A theory for fatigue failure under multiaxial stress-strain conditions," *Proc. Inst. Mech. Eng.*, vol. 187, no. 1, pp. 745–755, Jun. 1973.

[9] C. D. Lykins, S. Mall, and V. Jain, "A shear stress-based parameter for fretting fatigue crack initiation," *Fatigue Fract. Eng. Mater. Struct.*, vol. 24, no. 7, pp. 461–473, Jul. 2001.

[10] C. D. Lykins, S. Mall, and V. K. Jain, "Combined experimental–numerical investigation of fretting fatigue crack initiation," *Int. J. Fatigue*, vol. 23, no. 8, pp. 703–711, Sep. 2001.

[11] M. P. Szolwinski, J. F. Matlik, and T. N. Farris, "Effects of HCF loading on fretting fatigue crack nucleation," *Int. J. Fatigue*, vol. 21, no. 7, pp. 671–677, Aug. 1999.

[12] W. N. Findley, "Fatigue of metals under combinations of stresses," *Trans. Amer. Soc. Mech. Eng.*, vol. 79, no. 6, pp. 1337–1347, 1957.

[13] D. Rangel, D. Erena, J. Vázquez, and J. A. Araújo, "Prediction of initiation and total life in fretting fatigue considering kinked cracks," *Theor. Appl. Fract. Mech.*, vol. 119, Jun. 2022, Art. no. 103345.

[14] C. Wang, K. Pereira, D. Wang, A. Zinovev, D. Terentyev, and M. A. Wahab, "Fretting fatigue crack propagation under out-of-phase loading conditions using extended maximum tangential stress criterion," *Tribol. Int.*, vol. 187, Sep. 2023, Art. no. 108738.

[15] Y. Dong, D. Zeng, P. Wu, L. Lu, H. Zhao, Y. Li, and L. Zou, "Study on fretting fatigue crack initiation of scaled railway axles in consideration of fretting wear," *Wear*, vols. 512–513, Jan. 2023, Art. no. 204545.

[16] Q. Deng, N. A. Bhatti, X. Yin, and M. A. Wahab, "The effect of a critical micro-void defect on fretting fatigue crack initiation in heterogeneous material using a multiscale approach," *Tribol. Int.*, vol. 141, Jan. 2020, Art. no. 105909.

[17] S. Han, C. Wang, S. Khatir, Y. Ling, D. Wang, and M. A. Wahab, "A deep neural network approach combined with findley parameter to predict fretting fatigue crack initiation lifetime," *Int. J. Fatigue*, vol. 176, Nov. 2023, Art. no. 107891.

[18] S. Han, S. Khatir, C. Wang, and M. A. Wahab, "An improved artificial neural network for the direct prediction of fretting fatigue crack initiation lifetime," *Tribol. Int.*, vol. 183, May 2023, Art. no. 108411.

[19] S. Han, S. Khatir, and M. A. Wahab, "A deep learning approach to predict fretting fatigue crack initiation location," *Tribol. Int.*, vol. 185, Jul. 2023, Art. no. 108528.

[20] M. B. Gorji, A. de Pannemaecker, and S. Spevack, "Machine learning predicts fretting and fatigue key mechanical properties," *Int. J. Mech. Sci.*, vol. 215, Feb. 2022, Art. no. 106949.

[21] Z. R. Zhou, M. Fiset, A. Cardou, L. Cloutier, and S. Goudreau, "Effect of lubricant in electrical conductor fretting fatigue," *Wear*, vol. 189, nos. 1–2, pp. 51–57, Oct. 1995.

[22] S. Naboulsi and S. Mall, "Fretting fatigue crack initiation behavior using process volume approach and finite element analysis," *Tribol. Int.*, vol. 36, no. 2, pp. 121–131, Feb. 2003.

[23] C. T. Tsai and S. Mall, "Elasto-plastic finite element analysis of fretting stresses in pre-stressed strip in contact with cylindrical pad," *Finite Elements Anal. Des.*, vol. 36, no. 2, pp. 171–187, Sep. 2000.

[24] S. S. Chen and W. M. Sun, "Research on fretting fatigue damage and its fatigue life influence factors of 45 steel," M.D. thesis, Zhejiang Univ. Technol., Hangzhou, China, (in Chinese), 2006.

[25] C. D. Lykins, S. Mall, and V. Jain, "An evaluation of parameters for predicting fretting fatigue crack initiation," *Int. J. Fatigue*, vol. 22, no. 8, pp. 703–716, Sep. 2000.

WEN ZHOU was born Zhejiang, China, in 1983. He received the bachelor's degree from Zhejiang Ocean University, Zhoushan, China, in 2005, and the master's degree in chemical process equipment from the Zhejiang University of Technology, Hangzhou, China, in 2008. He is currently a Senior Engineer with the Quzhou Special Equipment Inspection Center. His current research interests include the safety of special pressure equipment, automatic test equipment, and mechatronics.

JIANGANG YE was born in Zhejiang, China, in 1972. He received the B.S. degree from Hangzhou Dianzi University, China, in 2001. He is currently a Senior Engineer with the Quzhou Special Equipment Inspection Center. His current research interests include mechatronics and materials.

KUN MAO was born in Zhejiang, China, in 1988. He received the bachelor's degree in automation from Beijing Forestry University, Beijing, China, in 2010, and the master's degree in control science and engineering from the Beijing Institute of Technology, Beijing, in 2013. He is currently a Lecturer with the Faculty of Information Engineering, Quzhou College of Technology. His current research interests include information fusion and mechatronics.

ZHENJIE LIU was born in Zhejiang, China, in 1984. He received the master's degree in thermal energy from Central South University, China, in 2010. He is currently an Engineer with the Quzhou Special Equipment Inspection Center. His current research interests include energy and power.

SHANG XIA (Member, IEEE) was born in Zhejiang, China, in 1984. He received the bachelor's degree in automation from Zhejiang Sci-Tech University, in 2008. He is currently an Engineer with the Quzhou Special Equipment Inspection Center. His current research interests include the safety of pressure vessels and pressure pipes.